

OPTICAL AND SAR IMAGERY FOR MAPPING VEGETATION GRADIENTS IN BRAZILIAN SAVANNAS: SYNERGY BETWEEN PIXEL-BASED AND OBJECT-BASED APPROACHES

L. M. T. de Carvalho^{a,b,*}, M. M. Rahman^b, G. J. Hay^b, J. Yackel^b

^a Dept. of Forest Sciences, Federal University of Lavras, 37200-000 Lavras, Brazil – passarinho@dcf.ufla.br

^b Dept. of Geography, University of Calgary, T2N 1N4 Calgary, Canada – (lcarvalh, mmrahm, ghay, yackel)@ucalgary.ca

Commission VI, WG VI/4

KEY WORDS: Indeterminate boundaries, SegSAR, CART, ALOS-PALSAR, Landsat-TM, Cerrado Biome

ABSTRACT:

The objectives of this study were (a) to evaluate the suitability of SAR imagery for discriminating savanna physiognomies, (b) to combine SAR and optical imagery for achieving improved accuracy, and (c) to develop a hybrid approach based on pixels and objects to characterize gradients of vegetation density. We used imagery from the Phased Array L-band Synthetic Aperture Radar (PALSAR), as well as imagery from the Thematic Mapper (TM) sensor. The PALSAR image was acquired in September 5th 2007, in dual polarization (HH and HV) with an off-nadir viewing angle of 34.3°. The TM image was acquired in September 10th 2007. Preprocessing comprised standard georeferencing and corrections for terrain effects using orthorectified Landsat TM (Geocover) and SRTM as reference datasets. The SAR and TM images were respectively converted to normalized radar cross section σ^0 and reflectance using published calibration factors. Visual image interpretation was used as the reference pattern for evaluating segmentation and classification procedures. The area was manually partitioned into polygons representing different land cover classes. Image segmentation for the automatic extraction of vegetation patches was performed using the SegSAR algorithm. Results were then compared to the visually delineated polygons. Object's classification accuracy was used to select land cover classes that represented transitional areas for further per-pixels analysis. Per-object classifications and per-pixels regression were carried out using CART. Results showed that several land cover objects could not be accurately segmented nor classified using SAR data alone. However, the same objects were accurately delineated in an automatic way using the optical image. Objects classification was more accurate when both SAR and optical data were input to CART. Per-pixel characterization of tree cover gradients within selected transition objects was developed to describe land cover patterns in the study area.

1. INTRODUCTION

According to McIntosh (1967) sampling and analysis of continuous transitions in plant communities extend at least as far back as Ramensky (1930). In some cases, these ecological transitions between adjacent vegetation types appear as indeterminate boundaries at the scale levels normally used in remote sense based surveys. Representation and visualization of these complex features using Geographical Information Systems (GIS) has gained considerable attention in recent years (Burrough and Frank, 1996).

Two conceptual views of the 'real world' have been widely used to represent and visualize the Earth's surface using GIS. One of them considers the space as being composed by features with homogeneous internal properties and separated by sharp boundaries. This approach has been called the 'exact entity' conceptual model. In contrast, the other view assumes that the space is characterized by gradual variations of surface properties and that no sharp boundaries exist. This is called the 'continuous field' conceptual model (Burrough and McDonnel, 1998). Choosing one of the two approaches has important implications to information extraction and has been considered a fundamental aspect in geography (Mennis et al., 2000).

Real world phenomena are somewhere in between this rigid dichotomy and the choice between models will certainly lead to incomplete characterizations. Most researchers guide their choice by the nature of the phenomenon under investigation,

including properties of the target process, as well as the spatial and temporal scales in which the phenomenon manifests itself (Silván-Cárdenas et al., 2009). The exact entity conceptual model has predominated research on mapping and monitoring land cover. Recently, a framework has been proposed and increasingly used in mapping projects. This framework, known as GEOBIA – Geographic Object-Based Image Analysis (Hay and Castilla, 2008), is strongly tied to the exact entity model with a few contributions dealing with continuous transitions among landscape features. Recent studies have explored the mapping of land cover classes with indeterminate boundaries within GEOBIA. Lucieer et al. (2005) have developed a procedure based on texture segmentation to extract exact entities and quantify uncertainty. They suggest that the spatial distribution of uncertainty measures provides information about localization and extent of transition zones. In another study (Cheng et al., 2001), the authors propose the creation of three fuzzy object models to represent land cover classes with indeterminate boundaries based on both, spatial extent and thematic information. With these models, they developed a formalism to assign pixels to objects using either raster or vector data structures, as well as to define transition zones with pixels belonging to none of the defined land cover classes.

Previous studies consider the representation of transition zones from an object-based perspective. However, phenomena occurring at a certain scale might exhibit some classes with indeterminate boundaries, while others have sharp boundaries. In this paper, we address the problem of mapping indeterminate

* Corresponding author.

boundaries by combining pixel- and object-based approaches to model vegetation classes with indeterminate boundaries.

Optical remote sensing has been a major information source for operationally mapping and monitoring land cover classes in Brazil (Carvalho and Scolforo, 2008; Câmara et al., 2006). Nevertheless, a number of studies have demonstrated that atmospheric conditions may significantly hamper information extraction from optical images in tropical regions (Asner, 2001; Sano, 2007). For this reason, the use of SAR imagery is considered a promising alternative to complement the monitoring systems currently based on optical data (Shimabukuru et al., 2007). It is expected a crescent application of SAR images for large-scale vegetation studies due to relatively lower data costs and to the recent increase in data availability after various new systems were launched, e.g., ALOS PALSAR, TerraSAR-X, Cosmo e Radarsat II (Lucas et al., 2006). In this context, another purpose of this paper is to report on the combined use of optical and SAR images within a GEOBIA framework.

1.1 Objectives

The objectives of this study were (a) to evaluate the suitability of SAR imagery for discriminating savanna physiognomies, (b) to combine SAR and optical imagery for achieving improved accuracy, and (c) to develop a hybrid approach based on pixels and objects to represent gradients of vegetation density.

2. SITE AND DATA

2.1 Study Area

The Brazilian Biome called Cerrado is the second largest in the country covering approximately two million square kilometres. It has been considered an important biodiversity hotspot (Myers et al., 2000) due to the highest levels of species richness and endemism when compared to other savanna-like Biomes of the world. Although much concern has been raised by the international community over the destruction of Amazonia, this Biome is far better preserved and protected than the Cerrado. In the past 40 years, intensive colonization has converted more than 50% of the Cerrado's natural vegetation to other land uses, in contrast to 20% that has been reported for the rain forests in the Amazonia. Furthermore, legal protection granted within National or State Parks and nature conservation reserves represents less than 3% of the Cerrado area, compared to 19% of the Amazonia. Thus, appropriate mapping and monitoring strategies must be urgently developed to guide sustainable management and conservation plans.

Natural vegetation in the Cerrado Biome varies from grasslands to dense forests. Commonly used classification systems (Veloso et al., 1991) include physiognomies called *campo limpo* (savanna grassland), *campo sujo* (mainly grass with scattered shrubs), *campo cerrado* (savanna park), *cerrado* (savanna sensu strictu), *cerradão* (savanna woodland), *vereda* (wet lands dominated by palm trees), and enclaves of Atlantic Forests (Carvalho 2008). Except for the very dense formations (*cerradão*, *vereda* and forest enclaves), boundaries between patches of different physiognomies are essentially indeterminate. These boundaries are characterized by a gradient of tree cover and biomass sometimes spanning hundreds of meters, which represent challenges to the definition of appropriate mapping methods.

The study site is located in the North of Minas Gerais, Brazil,

within the municipality of Cônego Marinho and bounded by the southern latitudes 14° 48' 28" and 15° 05' 02", and western longitudes 44° 42' 38" and 44° 25' 27" (Figure 1). The predominant vegetation physiognomies are *cerrado* and *campo cerrado*, interspersed with a few *vereda* patches. Most of the area is on a flat plateau with altitudes around 800 m. Land use is characterized by animal husbandry and localized agriculture. Besides, areas of impoverished vegetation occur due to cattle grazing and selective logging for charcoal production.

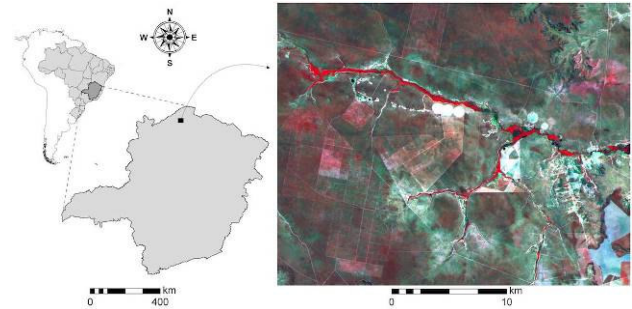


Figure 1. Location of the study area in Minas Gerais, Brazil.

2.2 Imagery and Pre-processing

Imagery from the Phased Array L-band Synthetic Aperture Radar (PALSAR) and the Thematic Mapper (TM) sensors were used in this study. The PALSAR image was acquired in September 5th 2007, in dual polarization (HH and HV) with an off-nadir viewing angle of 34.3°. The TM image was acquired in September 10th 2007.

Standard georeferencing and corrections for terrain effects using orthorectified Landsat TM (Geocover) and SRTM as reference datasets were conducted prior to image segmentation and classification. The SAR image was converted from amplitude data to normalized radar cross-section σ^0 and the TM image was converted to apparent reflectance. Both conversions were based on published calibration factors. Additionally, the PALSAR image was resampled to 30m to match the spatial resolution of the TM image.

2.3 Reference Data and Image Transforms

Visual interpretation of a high spatial resolution Ikonos image was used as the reference pattern for evaluating segmentation and classification procedures. The whole study area was partitioned by an experienced interpreter (Figure 2) who delineated polygons representing the following land cover classes occurring within the study area: Bare Land, *Campo Cerrado*, *Degraded Campo Cerrado*, *Cerrado*, *Degraded Cerrado*, and Wet Land.

It should be noted that visual interpretation of land cover classes with indeterminate boundaries, like transitions between *Cerrado* and *Campo Cerrado*, is also uncertain. Hence, polygons visually delineated for these classes were not considered when evaluating segmentation performance. On the other hand, wet and bare lands, as well as areas of degraded vegetation were clearly distinguishable on the high-resolution images as illustrated in Figure 3.

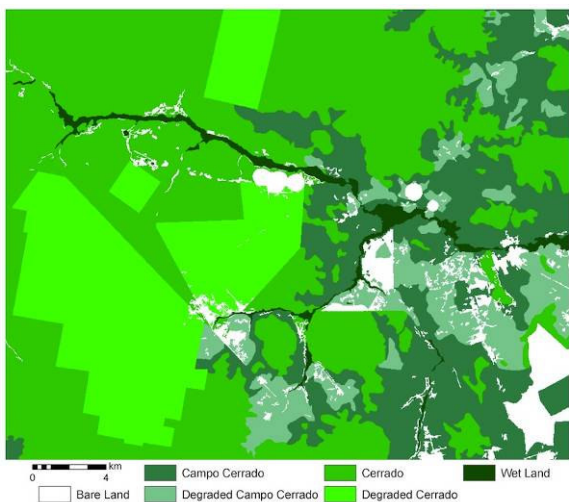


Figure 2. Reference map derived from visual interpretation.

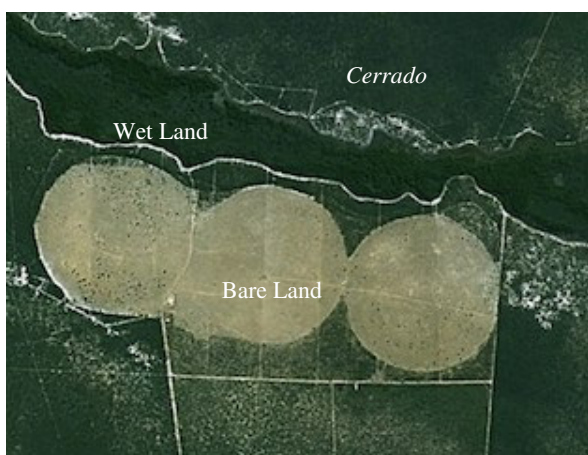


Figure 3. Subset of Ikonos image used for visual interpretation

A number of traditional transformations were applied to the PALSAR and TM images to investigate their potential to improve classification performance. In order to remove noise from the PALSAR image, two filtering procedures were implemented: the ‘à trous’ undecimated wavelet transform (Holschneider et al., 1989) was used to generate four approximation images at increasing scale levels; the Enhanced Lee Filter (Lopes, 1990) was applied to produce a speckle-reduced SAR images. From the TM image, the following transformations were computed: the Normalized Difference Vegetation Index (NDVI); linear spectral unmixing of soil, vegetation, and shadow fractions; and Tasseled Cap brightness, greenness, and wetness indices.

3. OBJECT-BASED IMAGE PROCESSING

3.1 Image Segmentation

The SegSAR algorithm (Souza, 2005) was used to extract image objects from both PALSAR and TM images. This algorithm was selected after preliminary tests evidenced its good performance for segmenting SAR images when compared to commercially available segmentation software. SegSAR is a hybrid approach to multiband image segmentation based on a combination of image compression, region growing, region grouping, and edge detection algorithms. It can also run two contrasting models based either on region homogeneity (cartoon

model) or heterogeneity (texture model) tests. Although originally developed and well suited to process SAR images, the software includes routines to segment optical images as well. In both cases, segmentation starts on the image at the highest compression level using automatically generated similarity thresholds. Then, tests for edge detection, region homogeneity/heterogeneity, and region grouping are performed at each compression level until the original uncompressed image is reached. The algorithm ends by testing if each region is larger than the user defined minimum segment area. The fundamental difference between SAR and optical image segmentation is related to the homogeneity/heterogeneity test. For SAR images, a critical test value is automatically obtained from the image’s Gamma distribution, whereas for optical images the user must provide this parameter. Reasonable segmentation outputs were obtained using the standard settings (Table 1) suggested by the software developer, Dr. Souza (pers. comm.), for segmenting the PALSAR and the TM images.

Parameter	PALSAR	TM
Compression levels	6	6
Model	Cartoon	Cartoon
Minimum area	20 pixels	20 pixels
Critical value	auto	0.30

Table 1. SegSAR settings used in this study.

In order to evaluate object extraction from optical and RaDAR images using SegSAR, we intersected polygons derived from manual delineation and the ones obtained automatically. Then, the best segmentation result based on visual inspection was selected for further processing.

3.2 Computation of Object’s Attributes

Attributes related to shape and area were calculated for each segmented polygon (Table 2). Polygons were also characterized by attributes derived from statistical measures of their pixel values (Table 3) in each image band, as well as in each transformation listed in section 2.3. Thus, 366 attribute variables were derived for each polygon.

Attribute Name	Attribute Name
Border Index	Length
Area	Rectangular Fit
Roundness	Radius of Smallest Enclosing Ellipse
Compactness	Density
Shape Index	Elliptic Fit
Main Direction	Asymmetry
Radius of Largest Enclosed Ellipse	Width
Length/Width	Border Length

Table 2. Attributes related to shape and area (Definiens 2007).

Attribute Name	Attribute Name
Mean	GLCM Entropy
Gray Level Co-occurrence Matrix (GLCM) Mean	GLDV Entropy
Gray Level Difference Vector (GLDV) Mean	GLCM Contrast
Standard Deviation	GLDV Contrast
GLCM Standard Deviation	GLCM Dissimilarity
GLCM Angular 2 nd Moment	GLCM Correlation
GLDV Angular 2 nd Moment	GLCM Homogeneity

Table 3. Attributes related to pixel values (Definiens 2007).

3.3 Data Mining and Classification

Due to the large number of attributes available to the classification process, data mining tools were used to select the ones providing the best separation among different land cover classes. Object based data mining and classification were

performed using a decision tree approach based on CART – Classification And Regression Trees (Breiman et al., 1984).

Data mining and classification with CART starts from a set of examples (i.e., training objects) described by a set of attributes (366 in this study). A binary decision rule is defined to split the set of image objects into subsets more homogeneous than the original one. Each subset is then subject to a new split generating even more homogeneous (sub-)subsets. Theoretically, the procedure iterates until ‘pure’ subsets are obtained. Decision rules at each split were obtained by thresholding the best discriminant attribute (Brodley and Utgoff, 1995). The final subset containing the best discriminant attributes is an indicator of variable importance and a way of discovering knowledge from highly dimensional decision spaces (i.e., data mining). The choice of attributes to be used in each split was guided by a quality measure – the GINI index of diversity – applied to the generated subsets. Final classification trees were selected based on the minimum error cost, which indicates the optimal relationship between tree size and classification errors based on cross-validation (Breiman et al., 1984). Image segmentation with SegSAR generated a total of 5486 image objects. From these, 964 samples were selected to compose the training set (Table 4).

Land cover class	Number of samples
Bare Land	215
<i>Campo Cerrado</i>	98
<i>Cerrado</i>	209
<i>Degraded Campo Cerrado</i>	53
<i>Degraded Cerrado</i>	176
Wet Land	213

Table 4. Description of training samples.

Three sets of attributes were input to data mining and classification to evaluate the effects of including information derived from SAR imagery for discriminating land cover classes. Firstly, a model was constructed using all shape attributes and attributes derived from the optical image. This feature set was composed by 198 attributes and called ‘shape+optical’. Then, a second model was constructed using all shape attributes and attributes derived from the SAR image, resulting in a set called ‘shape+radar’ composed by 184. Finally, the last model was adjusted considering all 366 variables derived from shape, optical and SAR attributes. This last set was called ‘shape+optical+radar’.

4. PIXEL-BASED IMAGE PROCESSING

4.1 Tree Cover Estimation

Polygons classified as *Cerrado*, *Campo Cerrado* and their respective degraded classes were selected to be further processed using a pixel-based approach. This approach was intended to evaluate the continuous characterization of vegetation areas, since thematic mapping of these areas proved inaccurate with considerable confusion among savanna physiognomies. The model developed by Tonelli (2008) for an area encompassing the present study site was used to estimate continuous fields of savanna tree cover. Tonelli’s model was also adjusted using decision trees, but this time in regression mode (Breiman et al., 1984). Regression with decision trees is similar to classification, but instead of outputting categorical information (e.g., land cover classes), the outputs are composed by continuous variables (e.g., percentage tree cover). The author mapped tree crowns on high spatial resolution Ikonos images and adjusted regression models to describe the relationship

between reflectance values observed on pixels of medium spatial resolution TM images and the respective mapped tree crown cover. This procedure has been successfully used to map tree cover and impervious surfaces at global scale levels (DeFries et al., 2000; Hansen et al., 2003).

5. RESULTS AND DISCUSSION

5.1 Image Segmentation

TM bands 1 to 5, and 7; as well as PALSAR HH and HV; Wavelet transformed PALSAR HH and HV; and Lee filtered PALSAR HH and HV were input to SegSAR, thus generating four segmented images. Segmentation results are illustrated in figure 4. Polygons automatically extracted from the optical image (Figure 4a) were selected for further processing because of better agreement with reference polygons. Segmentation evaluation was performed comparing a number of Wet Land and Bare Land areas from the reference map with the outputs of SegSAR. In all cases, the pattern shown in figure 4 was confirmed. Smoothing with wavelets (Figure 4c) and filtering with the Enhanced Lee filter (Figure 4c) provided no significant improvements over the segmentation of unprocessed PALSAR images (Figure 4b).

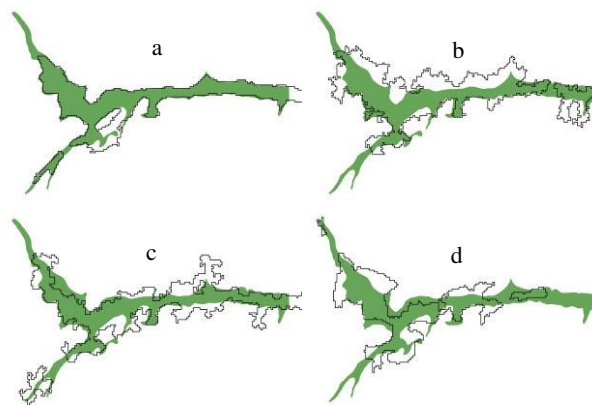


Figure 4. Results of image segmentation using SegSAR.

5.2 Object Based Image Classification

Three decision tree models were adjusted according to the available attribute sets, viz., shape+radar (184 attributes), shape+optical (198 attributes), and shape+optical+radar (366 attributes).

The shape+radar model was created with 12 nodes and a relative error cost of 0.536. Before pruning, the original tree was composed by 166 nodes and showed a relative error cost of 0.606. Cross validation produced 89.63% of overall correct classification for this model adjustment.

The shape+optical model was created with 16 nodes and a relative error cost of 0.144. Before pruning, the original tree was composed by 38 nodes and showed a relative error cost of 0.189. Cross validation produced 98.03% of overall correct classification for this model adjustment.

The shape+optical+radar model was created with 7 nodes and a relative error cost of 0.148. Before pruning, the original tree was composed by 36 nodes and showed a relative error cost of 0.191. Cross validation also produced 98.03% of overall correct classification for this model adjustment.

Properties of decision tree adjustments as described above give valuable information regarding classification performance. For

instance, it is clear that classification using solely attributes derived from polygons shape attributes and radar data values was more complicated. This fact is evidenced by the very large initial tree created before pruning (166 nodes) and also by the higher final error cost (0.536). It indicates that the provided set of attributes provided lower discrimination power when compared to the other two sets of attributes.

Classification performance was also evaluated using standard error matrices (Appendix) derived by the comparison of each resulting classification map and the reference map (Figure 5). Note that land cover classes with sharp boundaries, like Wet Land and Bare Land, were well depicted using object-based classification. In contrast, the spatial pattern of savanna distribution was not characterized properly.

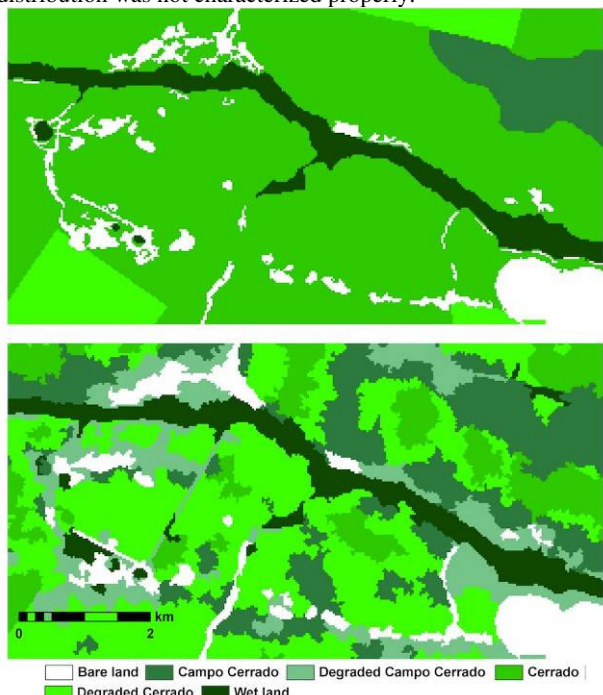


Figure 5. Reference image (top) and the most accurate classification map (bottom).

The performance for classifying savanna physiognomies is also evident in table 5 by looking at class mapping accuracies (Kalensky and Scherk, 1975). The best classification map according to overall accuracy and Kappa coefficient was the map produced using the ‘shape+optical+radar’ attribute set (Table 5). In this map, Degraded Cerrado and Degraded Campo Cerrado showed the lowest accuracies, whereas Bare and Wet lands the highest. These figures might be reflecting the complexity of transition zones among savanna physiognomies, as well as differences in degradation intensity. On the other hand, Bare and Wetlands were mapped with higher accuracies probably due to their shaper boundaries aiding segmentation and distinct reflectance properties, specially in areas of Bare Land.

	shape+ radar	shape+ optical	shape+ optical+radar
Overall accuracy	34.82	57.51	59.56
Kappa	18.53	45.53	47.69
Bare Land	18.04	48.11	65.40
Campo Cerrado	18.73	39.46	43.63
Degr. Campo Cerrado	16.99	27.19	31.19
Cerrado	25.85	48.72	49.25
Degr. Cerrado	28.03	36.88	35.71
Wetland	20.90	58.15	56.43

Table 5. Classification accuracy measures (%).

5.3 Importance of Object’s Attributes

From the 366 attributes derived in this study, data mining with decision trees indicated, in order of importance, the ones providing the best discrimination among land cover classes. Table 6, 7, and 8 show the importance measures derived from data mining with CART. Ranking was based on primary splitters (i.e., attributes actually used within tree nodes) that scored 10 or higher.

Attribute	Score
GLCM Homogeneity from TM band 4	100.00
Mean value from TM band 2	94.20
Mean NDVI value	87.59
Mean value from TM band 3	63.50
GLCM Homogeneity from TM band 7	53.56
GLDV Entropy from TM band 3	12.58
Mean value from TM band 7	11.64
Standard deviation value from TM band 2	11.35

Table 6. Importance of attributes from set ‘shape+optical’.

Attribute	Score
GLDV Entropy from HH	100.00
Mean value from 1 st scale Wavelet HH	74.70
Standard deviation value from HV	49.32
GLCM Mean value from 2 nd scale Wavelet HV	19.67
Mean value from Lee filtered HH	18.68
GLDV Angular 2 nd moment from 1 st scale Wavelet HV	17.96
GLCM Standard deviation from HV	14.02
Mean value from HH	11.68
GLCM Mean from 1 st scale Wavelet HH	11.38

Table 7. Importance of attributes from set ‘shape+radar’.

Attribute	Score
GLCM Homogeneity from TM band 4	100.00
Mean value from TM band 2	94.20
Mean NDVI value	87.59
Mean value from TM band 3	63.50
GLCM Homogeneity from TM band 7	53.56
GLDV Entropy from TM band 3	12.58

Table 8. Importance of attributes from set ‘shape+optical+radar’.

The six most important attributes in tables 6 and 8 are exactly the same. This means that the inclusion of radar attributes provided little or no improvement for discriminating among land cover classes in this study. Likewise, shape and area attributes were not used as predictors in any adjusted model. This type of information is probably most important to characterize anthropogenic features such as the ones found in urban and agricultural areas.

The presence of TM band 4 as the most important attribute, TM band 2 in second place, followed by the NDVI, shows the superior class separation provided by attributes related to reflectance values in the visible and near infrared regions of the electromagnetic spectrum. These results agree with axioms of remote sensing which state the importance of visible and near infrared energy for characterizing vegetated areas. Additional support is provided by the importance of basic statistical descriptors like means and standard deviations of visible and near infrared reflectance.

Texture measures derived from GLCM and GLDV showed the highest importance scores when using optical and SAR data respectively. GLCM Homogeneity is a measure of the overall smoothness and similarity of pixels within objects. Our results showed that these measures were useful for quantifying internal continuity in objects' reflectance variations. Entropy was important when considering SAR attributes. It measures disorder or complexity of the elements in the GLCM and seems to be correlated with differences in SAR backscatter of the land cover classes considered in this study. Finally, the importance of noise reduction provided by wavelet transforms was also verified.

5.4 Tree Cover Map

Image objects that could not be resolved at the present scale level were selected to be modelled with regression trees. Figure 6 illustrates the proposed combination of classes modelled using an object-based approach (Wet and Bare lands), as well as using a pixel-based approach (Cerrado Tree Density). This procedure provided a better characterization of transition zones within savanna physiognomies. Further research is being initiated to relate the patterns modelled here to biomass spatial distribution determined from field and LiDAR sampling.

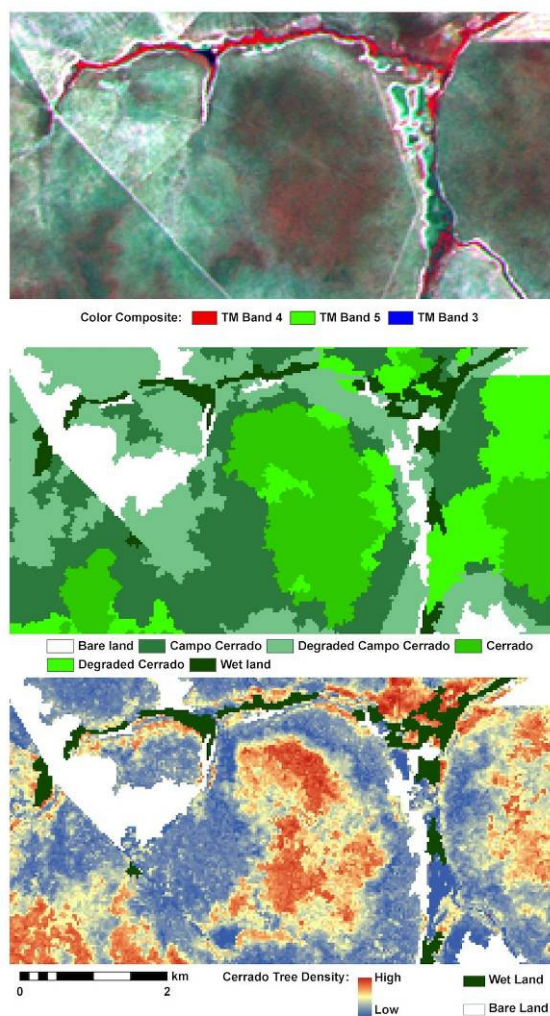


Figure 6. TM colour composite (top), best object-based classification (middle), and pixel-based regression (bottom).

6. CONCLUSIONS

The following statements could be derived from this study:

- SAR images did not provide accurate segmentation of objects with sharp boundaries within the savanna physiognomies studied.
- Classification accuracy was not enhanced by including SAR images nor any of its the transforms.
- Transitions between savanna physiognomies were properly characterized using continuous fields of tree cover.
- Models of continuous distribution of vegetation cover need to be validated with detailed biomass measurements.

7. REFERENCES

- Asner, G.P. 2001. Cloud cover in Landsat observations of the Brazilian Amazon. *International Journal of Remote Sensing*, 22, pp. 3855–3862.
- Breiman, L., Friedman, J. H., Olsen, R. A., Stone, C. J., 1984. *Classification and Regression Trees*. Wadsworth, Belmont, 368p.
- Brodley, C. E.; Utgoff, P. E. 1995. Multivariate decision trees. *Machine Learning* 19, pp. 45-77.
- Burrough, P. A.; McDonnell, R. A., 1998. *Principles of Geographic Information Systems*. Oxford University Press, New York, 356p.
- Câmara, G.; Valeriano D. M.; Soares, J. V. 2006. Metodologia para o Cálculo da Taxa Anual de Desmatamento na Amazônia Legal. São José dos Campos, INPE. 24p.
- Carvalho, L. M. T.; Scolforo, J. R. S. 2008. *Inventário Florestal de Minas Gerais - Monitoramento da Flora Nativa 2005-2007*. Lavras, Editora UFLA, v. 1. 357p.
- Cheng, T.; Molenaar, M.; Lin, H. 2001. Formalizing fuzzy objects from uncertain classification results, *International Journal of Geographical Information Science*, 15(1), 27-42.
- Definiens 2007. *Devolor 7.0: User Guide*. Definiens A G, München. 195p.
- DeFries, R. S., Hansen, M. C., Townshend, J. R. G., Janetos, A. C., Loveland, T. R. 2000. A new global 1-km dataset of percentage tree cover derived from remote sensing. *Global Change Biology*, 6, 247-254.
- Hansen, M.C., Defries R.S., Townshend, J.R.G., Sohlberg, R.A., Dimiceli, C., Carroll, M. 2002. Towards an operational MODIS continuous field of percent tree cover algorithm: Examples using AVHRR and MODIS data. *Remote Sensing of Environment*, 83, pp. 303–319.
- Hay, G. J.; Castilla, G. 2008. Geographic Object-based Image Analysis (GEOBIA): A new name for a new discipline. In: Blaschke T., Lang S., Hay G.J. (eds.) *Object-based Image Analysis: Spatial concepts for knowledge-driven remote sensing applications*. Springer-Verlag, Berlin.
- Holschneider, M.; Kronland-Martin, R.; Morlet, J.; Tchmitchian, P., 1989. A real time algorithm for signal analysis with the help of the wavelet transform. In: Combes JM, Grossman A, Tchmitchian P (eds.), *Wavelets: Time Frequency Methods and Phase Space*, Springer-Verlag, New York, pp. 286-297.
- Kalensky, Z. D., Scherk, L. R. 1975. Accuracy of forest mapping from Landsat CCTs. In: *Proceedings of the 10th International Symposium on Remote Sensing of Environment*, ERIM, Ann Arbor, 1159-1163.
- Lopes, A.; Touzi, R.; Nezry, E. 1990. Adaptive speckle filters and scene heterogeneity. *IEEE Trans. Geosc. Remote Sensing*, 28(28), pp. 992-1000.
- Lucas, R.; Lee, A.; Williams, M. 2006. Enhanced simulation of radar backscatter from forests using LiDAR and optical data, *IEEE Transactions on Geoscience and Remote Sensing* 44(10) pp.2736-2754.
- Lucieer, A.; Stein, A.; Fisher, P. 2005. Multivariate texture-based segmentation of remotely sensed imagery for extraction of objects and their uncertainty, *International Journal of Remote Sensing*, 26(14),

2917-2936.

Mennis, J.L., Peuquet, D.J. and Qian, L., 2000. A conceptual framework for incorporating cognitive principle into geographical database representation. *International Journal of Geographical Information Science*, 14(6), pp. 501–520.

Myers, N.; Mittermeier, R. A.; Mittermeier, D.; Fonseca, G. A. B.; Kentand, J. 2000. Biodiversity hotspots for conservation priorities. *Nature* 403, pp. 853-858.

Sano, E. E., Ferreira, L. G., Asner, G. P. and Steinke, E. T. 2007. Spatial and temporal probabilities of obtaining cloud-free Landsat images over the Brazilian tropical savanna, *International Journal of Remote Sensing*, 28(12), 2739–2752.

Shimabukuro, Y. E.; Almeida-Filho, R.; Kuplich, T. M.; Freitas, R. M. 2007. Quantifying optical and SAR image relationships for tropical landscape features in the Amazônia, *International Journal of Remote Sensing*, 28(17), pp. 3831-3840.

Silvan-Cardenas, J. L., Wang, L. and Zhan, F. B. 2009. Representing geographical objects with scale induced indeterminate boundaries: A neural network-based data model, *International Journal of Geographical Information Science*, 23(3), pp. 295-318.

Sousa Jr, M. A., 2005. *Segmentao multi-nveis e multi-modelos para imagens de radar e pticas*. Tese Doutorado em Computao Aplicada, Instituto Nacional de Pesquisas Espaciais, 133p.

Tonelli, C. A. Z. 2008. Estimativa da cobertura arborea utilizando a combinao de imagens Iknos e Landsat. Dissertao de Mestrado em Engenharia Florestal, Universidade Federal de Lavras, 133p.

Veloso, H. P., Rangel Filho, A. L. R., Lima, J. C. A. 1991. Classificao da vegetao brasileira, adaptada a um sistema universal. Rio de Janeiro, IBGE.

8. ACKNOWLEDGEMENTS

This study was financed by CNPq under grant PDE 202048/2008-0. Travel support for attending GEOBIA 2010 was provided to the first author by FAPEMIG. The authors are also grateful to Dr. Manoel de Araujo Souza Jr. for kindly providing access and consultancy related to SegSAR.

9. APPENDIX

	Reference Map						Total(%)
	BL	CA	Deg.CA	CE	Deg.CE	WL	
BL	77.87	1.7	5.17	0.42	0.39	0.21	5.29
CA	0.25	60.85	23.48	9.48	10.2	3.77	20.78
Deg.CA	20.93	20.25	64.65	3.37	9.89	2.17	14.01
CE	0.01	2.27	0.41	51.55	8.53	0.02	25.28
Deg.CE	0.41	12.49	2.81	34.43	70.81	3.83	31.65
WL	0.52	2.43	3.46	0.75	0.18	89.99	2.98
Total(%)	100	100	100	100	100	100	100

Table 9. Confusion matrix from classification ‘shape+optical+radar’.

	Reference Map						Total(%)
	BL	CA	Deg.CA	CE	Deg.CE	WL	
BL	75.97	5.75	11.87	1.29	2.13	0.98	7.3
CA	5.56	52.95	20.1	7.64	8.88	1.96	18.05
Deg.CA	17.53	25.15	61.45	5.01	9.54	3.21	15.28
CE	0.01	2.32	0.41	50.55	6.26	0.02	24.42
Deg.CE	0.41	11.64	2.78	34.79	73.1	3.83	32.06
WL	0.52	2.19	3.4	0.71	0.08	89.99	2.89
Total(%)	100	100	100	100	100	100	100

Table 10. Confusion matrix matrix from classification ‘shape+optical’.

	Reference Map						Total(%)
	BL	CA	Deg.CA	CE	Deg.CE	WL	
BL	47.96	15.09	16.35	8.25	3.5	11.03	11.66
CA	33.15	41.54	30.96	35.05	26.86	5.66	33.84
Deg.CA	14.17	19.05	38.49	9.5	6.65	4.14	13.46
CE	1.21	11.77	5.45	30.31	25.22	4.72	21.39
Deg.CE	0.8	2.23	5.45	11.44	37.17	0.02	13.05
WL	2.71	10.31	3.3	5.44	0.61	74.42	6.6
Total(%)	100	100	100	100	100	100	100

Table 11. Confusion matrix matrix from classification ‘shape+radar’.